Food Chemistry 398 (2023) 133903

Contents lists available at ScienceDirect

Food Chemistry

journal homepage: www.elsevier.com/locate/foodchem

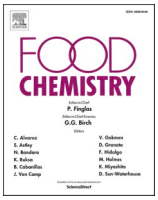

Glutathione metabolism-mediated ferroptosis reduces water-holding capacity in beef during cold storage

Jun Liu [a], Ziying Hu [b], Dunhua Liu [a,b,*], Anran Zheng [a], Qin Ma [b]

[a] School of Agriculture, Ningxia University, 750021 Yinchuan, China
[b] School of Food & Wine, Ningxia University, 750021 Yinchuan, China

ARTICLE INFO

Keywords:
Ferroptosis
Metabolomic
Beef
Exudate
Water-holding capacity

ABSTRACT

To investigate the potential mechanisms by which cold storage affects the water-holding capacity (WHC) of beef through analysis of exudates using an untargeted metabolomics strategy. A total of 877 metabolites were detected in four groups of beef exudates that have been frozen for 1, 2, 4, and 6 days, of which, 278 were identified as differential metabolites (DMs). The metabolic pathways of the DMs analysed by KEGG pathway enrichment included ABC transporters, purine metabolism, biosynthesis of cofactors, protein digestion and absorption, and ferroptosis. Ferroptosis was identified during storage of beef, and the reduction in WHC of beef was accompanied by a ferroptosis process. In addition, six DMs were identified in the KEGG pathway of ferroptosis, and the process of cellular ferroptosis was dependent on the inhibition of glutathione metabolic processes. Overall, the ferroptosis of cells during beef storage had a negative impact on WHC, and the finding of ferroptosis complemented the post-slaughter apoptosis.

1. Introduction

The beef product is among the most valuable and in-demand meats currently available, and it is essential to assess its quality properly (Castejón et al., 2015). The moisture content is one of the most crucial factors affecting the organoleptic acceptability and economic value of meat products, meaning that the meat needs to maintain a high water-holding capacity (WHC) (Zhang et al., 2019; Kristensen & Purslow, 2001). Therefore, chilled beef is sold during the display period whenever possible (Karakaya et al., 2005). The loss of juices or exudate is a visual representation of reduced WHC, while changes occur at the physiological and molecular level in the muscles, when are converted into meat, and when they age, including decreased temperature after the immediate post-slaughter and pH value, apoptosis, a transformation from aerobic to anaerobic respiration, myofibrillar shrinkage and contraction, myosin denaturation, etc. (Cheng & Sun, 2008; Zhang et al., 2019).

The exudate includes both immobilized and free water, and contains a blend of haem (myoglobin or hemoglobin), nucleotides, peptides, amino acids, soluble enzymes, and water-soluble vitamins (Castejón et al., 2015). Exudates are usually unavoidable during the storage of fresh meat, accumulate on meat's surface, as well as in packaging boxes and bags, and can range from 1 % to 3 % (Xing et al., 2020). Correlations have been established between muscle exudates and the components of the exudates with meat characteristics, including freshness, tenderness, colour, WHC, lipid and protein oxidation, and microbial contamination (Bowker et al., 2016; Kim et al., 2013), indicating that assessing the profile of meat exudate may help understand changes in meat quality characteristics (Castejón et al., 2015). In conclusion, it is necessary to investigate the potential mechanisms affecting meat WHC, quality characteristics affected by WHC, or the formation of exudate (Kim et al., 2013).

The study aimed to determine the relationship between the metabolite composition and pathways of bovine muscle exudates and WHC during post-slaughter display. We collected exudate samples from 1, 2, 4, and 6 days of refrigeration and analyzed metabolite composition and metabolic pathways with an untargeted metabolomics strategy using UPLC-ESI-Q-Orbitrap-MS. The results of this study may help understand the mechanisms controlling quality attributes, and identify the potential for utilizing meat exudate as an easily accessible source of metabolite markers of beef quality.

* Corresponding author at: Room 320, College of Agriculture, Helanshan Campus, Ningxia University, No. 489, Mount Helan West Road, Xixia District, Yinchuan City, 750000 Ningxia, China.
E-mail addresses: dunhualiu@126.com, ldh320@nxu.edu.cn (D. Liu).

https://doi.org/10.1016/j.foodchem.2022.133903
Received 27 April 2022; Received in revised form 10 July 2022; Accepted 7 August 2022
Available online 10 August 2022

2. Materials and methods

2.1. Raw materials

Eight male yellow cattle from a farm in China (Qinchuan cattle, 18–24 months old, body weigh 400 ± 20 (SD) kg) were humanely killed at a local slaughterhouse in Ningxia (Yitai Herding Co., Yinchuan, China) according to the guidelines of the Canadian Council on Animal Care (CCAC) & The Assessment Program of the CCAC (2000). Following cattle exsanguination, a sample of approximately 500 g of *M. longissimus lumborum* muscles (loins) (from the twelfth thoracic vertebrae to the fifth lumbar vertebrae) was immediately obtained, placed in a polyethylene self-sealing bag in a foam box filled with ice packs, and a plastic divider in the middle, and transported to the laboratory within 3 h. The muscle samples were divided into four groups (n = 8) after being sliced into pieces with a thickness of 2.5 cm and an average weight of 100.0 ± 5.0 g. The muscles were put onto a PET plastic tray (length, 195 mm; height, 30 mm; width, 145 mm), and wrapped with polyvinyl chloride film. Muscles were displayed for 6 days at 4.0 ± 0.5 °C in an open-front refrigerated display case (XR150D, Foshan City Aslok Refrigeration Equipment Co., ltd., Foshan, China) with a single shelf and a 30-degree tilt at the bottom. Muscles were placed randomly and rotated twice daily to obtain random sample placement. All muscle exudates were collected from the bottom of the tray with a medical disposable syringe on the storage days 1, 2, 4, and 6, defined as EXU1, EXU2, EXU4 and EXU6. The exudates were stored in 2 mL lyophilisation tubes using liquid nitrogen for rapid freezing and rapidly transfered to a medical cryostat storage chamber (DW-86L486, Qingdao Haier Biomedical Co., Qingdao, China) at −80 °C. Muscle samples were taken from the center for meat quality, defined as Day 1, Day 2, Day 4, and Day 6, and fresh samples were used for meat quality analysis (Bowker et al., 2016; Chen et al., 2021; Liu et al., 2022).

2.2. Measurement of WHC

The purge loss (PL), drip loss (DL), and centrifuging loss (CL) were determined using our previous method (Liu et al., 2022). Briefly, PL was calculated as a percentage of weight loss in the beef under storage conditions at 4 °C. DL was determined as a percentage loss of beef weight derived from a 24-h hang-out at 4 °C. After centrifugation at a low speed of 1500×g for 5 min at 4 °C, CL was determined as a percentage of weight loss.

2.3. Low-field (LF) NMR relaxometry

The LF NMR technique was used to analyze changes in the moisture state of beef (Liu et al., 2022). The transverse relaxation time (T2) was determined on a NMI20 benchtop pulsed NMR analyzer (Niumag Electronic Technology Co., ltd., Shanghai, China). Three 5 × 0.75 × 0.75 cm strips of the sample were removed from each muscle in the direction of the fibres, then 2.0 ± 0.2 g of the sample were wrapped in a parafilm membrane and placed in a cylindrical glass tube (15 mm diameter) supplied with the instrument. The analyzer was operated at 25 °C at a resonance frequency of 18 MHz. Transverse relaxation (T2) was measured using a CarrPurcell-Mebiboom-Gill (CPMG) sequence with a τ-value of 200 μs. The samples were repeatedly scanned 16 times at 100 μs intervals and a total of 2000 echoes were collected. Data analysis was performed under the MultiExp Inv Analysis (Niumag Electronic Technology Co., ltd., Shanghai, China) project to fit the distributed exponential fitting of CPMG decay curves and obtain the T2.

2.4. Apoptotic nuclei detection and ROS fluorescent staining

Apoptosis was assessed by using the TUNEL Apoptosis In Situ Assay Kit (G002-1–2, Nanjing Jiancheng Biological Co., ltd., China). The paraffin-embedded muscle was made into 5 μm tissue sections, and the dewaxed samples stained according to the steps in the instructions provided by the manufacturer. The muscle tissue section was analysed for the number of positive nuclei using fluorescence microscopy imaging (TI2, Nikon Co., Tokyo, Japan), and at least three different fields of view (×200) were obtained for each sample. In the muscle tissue, apoptosis rates were calculated by comparing the number of positive nuclei to the total number of nuclei after staining the whole muscle. Reactive oxygen species (ROS) fluorescence staining was performed with reference to a previous method, and ROS content was expressed as fluorescence intensity (Liu et al., 2022).

2.5. Metabolomic analysis of exudate

2.5.1. Sample pretreatment

A sample of 100 μL of exudate was thoroughly mixed with 400 μL of cold methanol acetonitrile (*v/v*, 1:1). The mixture was sonicated for 1 h in an ice bath, then left to stand at −20 °C for 1 h, followed by centrifugation at 16,000×*g*, 4 °C for 20 min. Mass spectrometry was conducted on the supernatant.

2.5.2. UHPLC-MS/MS analysis

Metabolomics profiling was conducted using an UPLC-ESI-Q-Orbitrap-MS system (UHPLC, Shimadzu Nexera X2 LC-30AD, Shimadzu, Japan) coupled with Q-Exactive Plus (Thermo Scientific, San Jose, USA). For hydrophilic interaction liquid chromatography (HILIC) separation, samples were analyzed using a 2.1 mm × 100 mm ACQUIY UPLC BEH Amide 1.7 μm column (Waters Inc., Wexford, Ireland). The flow rate was 0.5 mL/min and the mobile phase consisted of 25 mM ammonium acetate and 25 mM ammonium hydroxide in water (A) and 100 % acetonitrile (B). The gradient was 95 % acetonitrile for 1 min and was linearly reduced to 65 % in 7 min, and then reduced to 35 % in 2 min and maintained for 1 min, and then increased to 95 % in 0.5 min, with a 2 min re-equilibration period.

Both electrospray ionization (ESI) positive- and negative - modes (POS and NEG) were applied for MS data acquisition. The HESI source conditions were set as follows: Spray voltage: 3.8kv (+) and 3.2kv (-); Capillary temperature: 320 (±); Sheath gas: 30 (±); Aux gas:5 (±); Probe heater temp: 350 (±); S-lens RF level: 50. In MS only acquisition, the instrument was set to acquire over the *m/z* range 80–1200 Da. The full MS scans were acquired at a resolution of 70,000 at *m/z* 200, and 17,500 at *m/z* 200 for MS/MS scan. The maximum injection time was set for 100 ms for MS and 50 ms for MS/MS. The isolation window for MS2 was set to 2 *m/z* and the normalized collision energy (stepped) was set as 27, 29 and, 32 for fragmentation.

2.5.3. Data preprocessing and multivariate statistical analysis

The raw MS data were processed using MS-DIAL (RIKEN, Yokohama, Japan) for peak alignment, retention time correction, and peak area extraction. The metabolites were identified by accuracy mass (mass tolerance <0.01 Da) and MS/MS data (mass tolerance <0.02 Da) which were matched with HMDB, public databases metabolite standard library. The discriminating metabolites were obtained using a statistically significant threshold of variable influence on projection (VIP) values obtained from the orthogonal partial least-squares discrimination analysis (OPLS-DA) model and two-tailed Student's *t* test (*P*-value) on the normalized raw data at univariate analysis level. The *P*-value was calculated by one-way analysis of variance (ANOVA) for multiple groups analysis. Metabolites with VIP values >1.0 and *P*-value <0.05 were considerred to be statistically significant metabolites.

The R language 'limma' package (R version 4.1.2, https://www.r-project.org/) was used for all multivariate data analyses, modeling, and cluster analyses. Data were mean-centered using Pareto scaling. Models were built on principal component analysis (PCA) and OPLS-DA. All the models evaluated were tested for over fitting with methods of permutation tests.

2.5.4. KEGG enrichment analysis

The differential metabolite data were subjected to KEGG pathway analysis using KEGG database (https://www.kegg.jp). KEGG enrichment analyses were carried out with the Fisher's exact test, and FDR correction for multiple testing was performed. Enriched KEGG pathways were nominally statistically significant at $P < 0.05$ level.

2.6. Isolation of myoblasts

Referring to the previous methods by Chen et al. (2022), Dong et al. (2022) and Xu, Huang, Zhu and Guo. (2022), fresh bovine muscle samples were sterilised in alcohol, rinsed in PBS and then placed onto petri dishes containing double anti-buffer solution. Microscissors were cut and placed in a centrifuge tube, centrifuged at 1500×*g* for 5 min, pipetted into a tissue suspension, and then the suspension was loaded into a 50 mL cell culture flask. For 30 min at room temperature, 0.25 % trypsin solution was used to dissociate the rest of the muscle tissue. Centrifugation was used to collect the cells and were eventually grown in DMEM/F12 medium (5 % equine serum protein, 1 μmol/L ferric citrate). The 10 μmol/L ferroptosis inducer erastin was added to the mixture, and the myoblasts-containing suspension collected by repeating the procedure.

2.7. Characterization of ferroptosis in myocytes

Apoptosis was detected by a Accuri C6 Plus flow cytometer (BD Biosciences, NJ, USA) according to the G003-1-3 Annexin V-FITC/PI double staining apoptosis detection kit instructions. Cells were resuspended in PBS, fragmented using an ultrasonic processor, the glutathione (GSH) content and glutathione peroxidase (GPx) activity were determined using the reduced GSH tissue kit and the GPx tissue kit. The content of myocyte ROS was measured using the ROS analysis kit and expressed as fluorescence intensity, and the level of malonaldehyde (MDA) was measured using MDA analysis kit (Jiancheng Biological Co., Nanjing, China).

2.8. Statistical analyses

Results were presented as the mean values of three independent experiments ± standard deviations (SD). Data were analysed one-way ANOVA, followed by post hoc LSD multiple range tests using IBM SPSS 25.0 software (SPSS Inc. NY, USA) ($P < 0.05$). Figures were created utilising Origin 2021b (OriginLab Co., MA, USA).

3. Results

3.1. Changes in WHC, apoptosis, and oxidation status of beef during display

As shown in Fig. 1a, PL increased as the display period increased, reaching a cumulative loss of 3.04 % in 6 d. Both DL and CL tended to increase from 1 d to 4 d, with the highest rate of loss at 4 d. The water distribution of the muscle was measured using LF NMR (Fig. 1b). Three different moisture states are generally present in meat, including bound water (T_{21}), immobilized water (T_{22}), and free water (T_{23}) (Li, et al., 2018). A decrease in the percentage of T_{21} and T_{22} and an increase in the percentage of T_{23} were observed with increasing storage time, indicating a decrease in mobile water and an increase in free water. Overall, these results showed that the WHC of beef decreased and water loss increased during display. As shown in Fig. 1c and d, the rate of apoptosis and ROS fluorescence intensity increased significantly ($P < 0.05$) with display time.

3.2. Identification of beef exudate metabolites

To identify beef exudate metabolites, an untargeted metabolic profiling was performed on four sets of samples using UPLC-Q-Exactive MS and Q-Exactive Plus (Table S1), which typically annotated 572 metabolites in the POS and 305 metabolites in the NEG. Analysis of multivariate data using PCA and OPLS-DA was used to obtain the variation of different metabolites in exudate during beef display. As shown

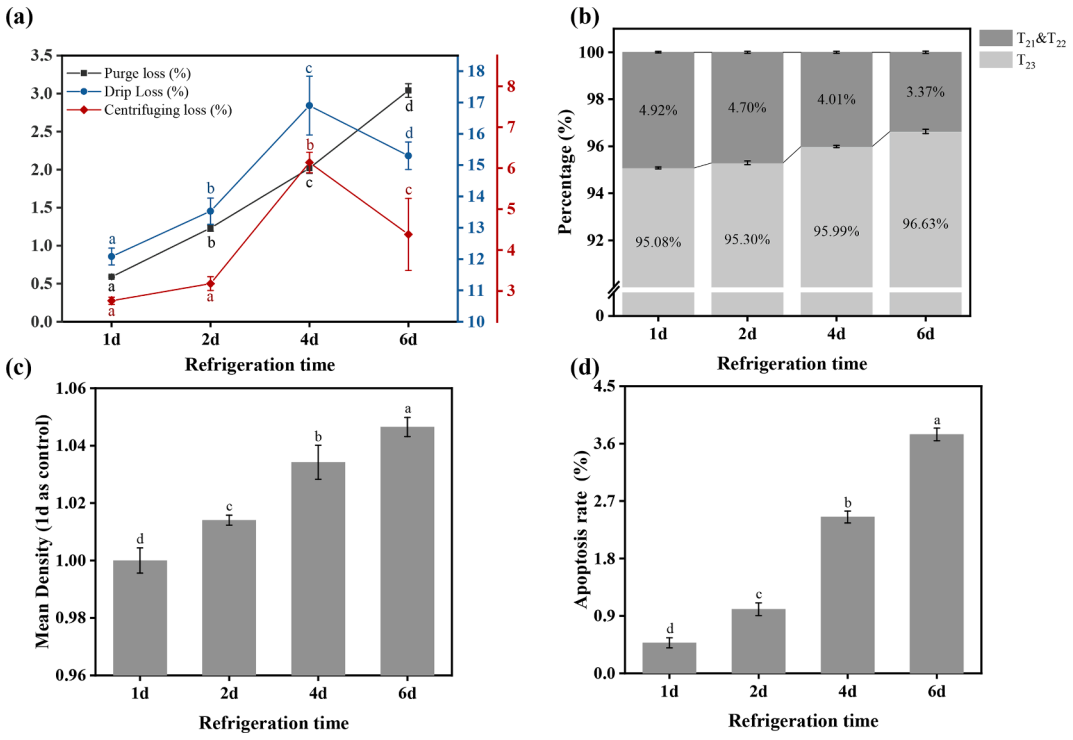

Fig. 1. (a) Changes in the WHC of beef during chilled. (b) Analysis of water distribution of beef during chilled by low-field NMR. (c) Fluorescence intensity of beef tissues stained with ROS during chilled. (d) Changes in the proportion of apoptotic nuclei (×200) in beef cells at during chilled. Significant differences exist among the different letters (a-d) ($P < 0.05$).

in Fig. 1a and b, the four exudates in POS and NEG were distinguished according to the first two principal components (PC1 and PC2). EXU1 and EXU2 were not completely separated in the four groups (Fig. 1a and b). The outcomes of PCA and OPLS-DA (Figure S1) indicate a reliable separation between the two, EXU 1/2 was well separated from EXU 4/6, and the longer the storage time of the beef, the higher the differentiation of the exudate from EXU1. These results indicated that the changes in metabolites tended to increase with storage time.

To better reflect the differences between the EXU1 and EXU 2/4/6 samples, after removing the QC samples, the samples were further analysed using OPLS-DA. The EXU1 and EXU 2/4/6 groups tended to cluster within groups and separate between groups in both POS and NEG, which was more evident in OPLS-DA (Fig. 1c). Fig. 1d and f show the model alignment test plots obtained from OPLS-DA after 200 rounds of interaction validation. In general, Q2 > 0.5 indicates good stability and reliability of the model. In the stochastic model, the R2 and Q2 decreased as the retention rate of permutations decreased, the original model did not show over-fitting and was reliable and robust. These results showed that the separation of metabolites between the EXU1 and EXU 2/4/6 groups as displayed by OPLS-DA was statistically significant, the model was reliable for screening marker metabolites (Fig. 1c, d, e, and f).

Afterwards, 278 metabolites were screened for significant differences from EXU1 using variable importance for the projection (VIP) > 1 and one-way ANOVA *t*-test $P < 0.05$ as screening criteria (Table S2), of which 114 and 164 metabolites were down- and up-regulated respectively. Hierarchical clustering was performed for each group of samples based on expression, and Fig. S2 shows the clustering heat map of the differential metabolites (DMs), with metabolites clustered within the same cluster having similar expression patterns. In addition, the KEGG data were used to classify the DMs into 29 superclasses, with different colours indicating different superclasses (Fig. S2), mainly including

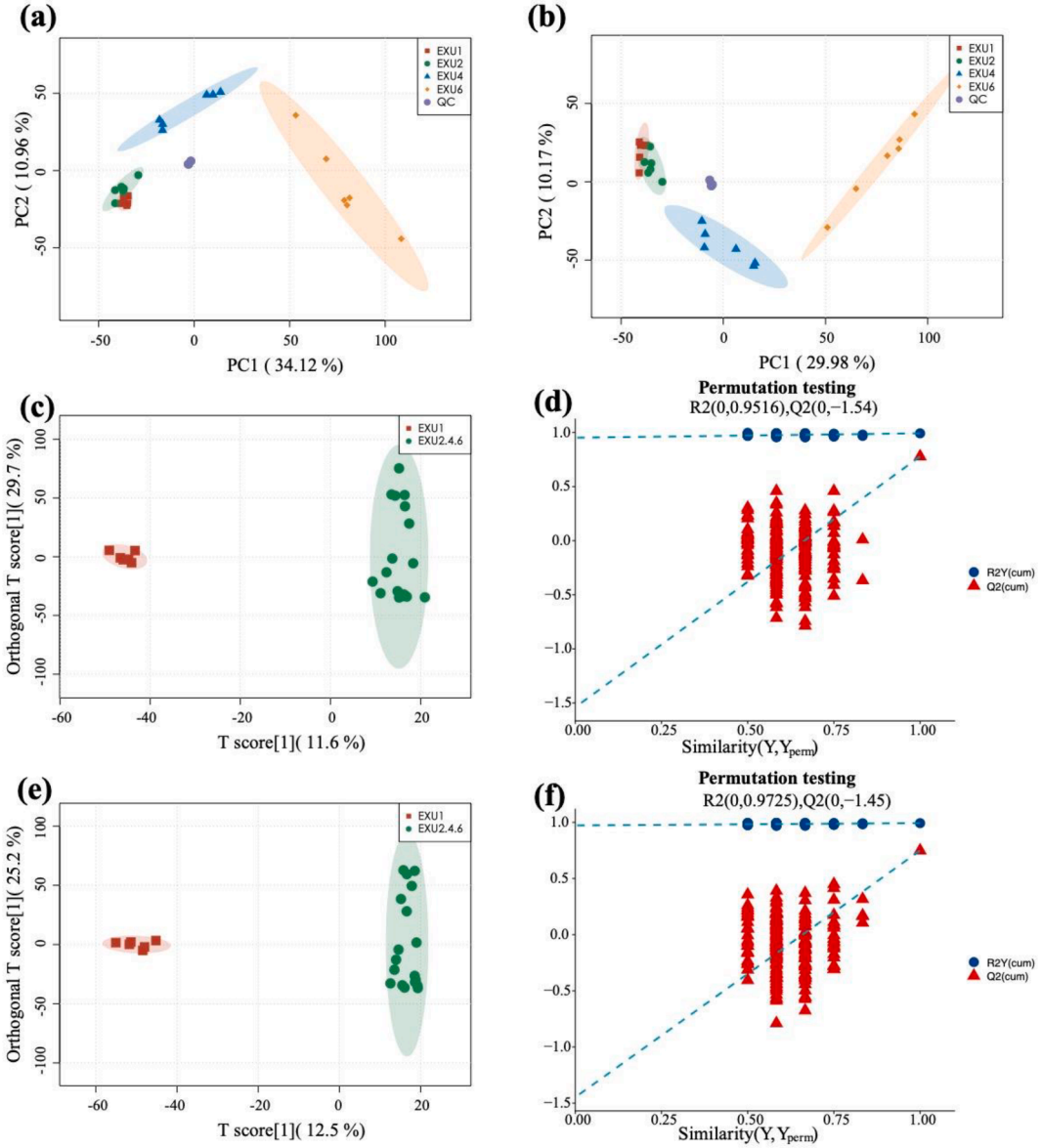

Fig. 2. Multivariate statistical analysis of identified metabolites in four groups of exudates. (a) PCA score plots of samples acquired in POS) (b) PCA score plots of samples acquired in NEG) (c) OPLS-DA score plots of samples acquired in POS. (d) The validation of the OPLS-DA model by permutation testing (200 iterations) in POS. (e) OPLS-DA score plots of samples acquired in NEG. (f) The validation of the OPLS-DA model by permutation testing (200 iterations) in NEG. EXU1, EXU2, EXU4, and EXU6 denote beef exudate samples from 1 d, 2 d, 4 d, and 6 d of storage respectively. QC in PCA denotes quality control reference samples. The horizontal coordinates in the OPLS-DA represent the correlation between Y of the random subgroup and the original subgroup Y. The vertical coordinates represent the scores of R2 and Q2, with R2 indicating the model explanatory rate and Q2 indicating the model predictive ability.

pesticides (14), alkaloids (11), nucleic acids (7), phenylpropanoids (6), pk polyketides (5), vitamins and cofactors (4), organic acids (4), carbohydrates (4), terpenoids (3), and lipids (3) (Fig. 2).

3.3. KEGG classification and enrichment analysis of the DMs

To better understand the variation of the major DMs in the exudate, the DMs obtained in the three comparison groups (EXU 1/2, EXU 1/4, EXU 1/6) were mapped to the KEGG database, and 39, 93, and 117 DMs with KEGG IDs were obtained and these DMs were grouped and counted (Fig. 3a, c, and e). The major DMs in the exudate were alkaloids, PK polyketides, vitamins and cofactors, peptides, phenylpropanoids, and FA fatty acyls. Further analysis of the metabolic pathways of the DMs by KEGG pathway enrichment (Fig. 3b, d, and f) has found ABC transporters, protein digestion and absorption, purine metabolism, biosynthesis of cofactors, ferroptosis, aminoacyl-tRNA biosynthesis, and biosynthesis of amino acids. Of note, tissue-dependent ferroptosis was identified in the EXU 1/4 and EXU 1/6 metabolic pathways (Fig. 3d and f).

3.4. DMs involved in ferroptosis

KEGG pathway enrichment analysis of EXU 1/4 and EXU 1/6 identified 5 and 6 DMs with KEGG ID involved in the ferroptosis process, respectively, including L-glutamic acid, arachidonic acid, glutathione (oxidized), L-cystine, gamma-glutamylcysteine and glutathione, of which 1 of EXU 1/4 DMs was upregulated, 4 were down-regulated; In the DMs of EXU 1/6, 2 were up-regulated and 4 were down-regulated. As shown in Fig. 5e and Fig. S3, these DMs may be dependent on glutathione metabolism for the regulation of cellular ferroptosis. To further explore the potential metabolic pathways involved in ferroptosis *via* glutathione metabolism, the KEGG-enriched metabolic pathway was conducted (Fig. 4g). Cellular processes include ferroptosis, necroptosis, and gap junction, in addition to involvement in ABC transporters, ROS, cysteine, methionine metabolism, and glutathione metabolism. A functional interaction network of these DMs involvement pathways was mapped using the KEGG enrichment pathway, with ferroptosis located in the middle of the diagram, suggesting that ferroptosis may be closely associated with multiple metabolic processes.

3.5. Erastin induced ferroptosis in myocytes

To verify the effect of glutathione metabolic pathways on ferroptosis in muscle cells, myocytes were incubated with the ferroptosis inducer, erastin, and key cellular characteristics of ferroptosis were determined. As shown in Fig. 5a and b, the early apoptotic rate (Q2) was 2.80 % and 3.84 %, and the late apoptotic rate (Q3) was 3.80 % and 9.36 % in the control and treat groups respectively. In Q2 and Q3, the control group did not show any significant difference ($P > 0.05$), and Q3 in the erastin-treated group was significantly higher than Q2 ($P < 0.05$). The results suggested that the ferroptosis inducer effectively induced ferroptosis in the myocytes. Furthermore, the cellular ferroptosis was accompanied by a reduction in GSH content and GPx activity (by 70.69 % and 56.81 % respectively, $P < 0.05$) (Fig. 5c). In addition, the concentrations of ROS and MDA were significantly higher ($P < 0.05$, Fig. 5d).

4. Discussion

Ferroptosis is a recently discovered mode of cell death triggered by intracellular iron overload. The hallmark event of the process is the inhibition of GPx 4 activity and the accumulation of ROS that cannot be efficiently removed, leading to lipid peroxidation within the cells (Xia et al., 2021). Iron ions, including ions, iron-sulphur clusters, myoglobin iron, haemoglobin iron, and ferritin are essential trace elements in animals and humans. However, iron ions use H_2O_2 as an electron donor, and ROS are generated at the Fe^{3+} and Fe^{2+} transition (Fenton reaction). Furthermore, the accumulation or enrichment of intracellular $Fe^{2+/3+}$ or inhibition of GPx4 accelerates the process of lipid peroxidation of fatty acids, which is the most typical feature of ferroptosis (Yang & Stockwell, 2016). In the study, 6 DMs associated with ferroptosis were identified, and 5 DMs may cause cellular ferroptosis by affecting the glutathione (GSH) metabolic pathway (Fig. 4). The mechanism of glutathione metabolic pathway-mediated ferroptosis is shown in Fig. 5e. L-glutamic acid, L-cystine, and γ-glutamylcysteine are important substances for GSH synthesis, cystine/glutamate antiporter (System Xc^-) undergoes a 1:1 transportation of L-glutamate for cystine, glutamate levels affect the function of System Xc^-, and higher extracellular concentrations of glutamate inhibit System Xc^- transport (Pitman et al., 2019), resulting in increased intracellular depletion of cysteine, a precursor to GSH synthesis. The accumulation of glutamate verified that System Xc^- function was inhibited (Fig. 4). Although cystine/glutamate can be interconverted intracellularly, the transport process from extracellular to intracellular is the underlying cause of the change in cysteine content (Hirayama & Nagasawa, 2017). Glutamate may also act as a signalling molecule (neurotransmitter), and its over-stimulation when present in excess near the cell may increase intracellular calcium (Ca^{2+}) by directly opening post-synaptic ion channels, cause mitochondrial damage and release apoptosis-inducing factor (AIF), which may in turn lead to a non-apoptotic cell death caused by oxidation, with many features of ferroptosis (Mehta et al., 2013; Yang & Stockwell, 2016). L-glutamic acid was found to be involved in the intercellular gap junction as a signalling molecule (Fig. 4g, Table S3), while the pathway-pathway interplay network suggests that L-glutamate acid may regulate cellular ferroptosis through its involvement in gap junction (Fig. 4h). Cystine can be reduced intracellularly to cysteine, which is implicated in GSH synthesis *via* the glutathione pathway (Fig. S3), an important antioxidant and free radical scavenger, and cysteine is considered to be the most important limiting factor for GSH synthesis (Bridges, Natale & Patel, 2012). Furthermore, cysteine deficiency resulted in hyperpolarization of the mitochondrial membrane potential and lipid peroxidation, suggesting that cysteine may induce ferroptosis in the cells *via* the mitochondrial pathway (Wang et al., 2020). Among other DMs, the level of γ-glutamylcysteine increased while the level of glutathione decreased, which may be related to the inhibition of glutathione synthase activity. The increase in γ-glutamylcysteine content was dependent on cysteine, which also contributed to the down-regulation of cysteine. GPx4 can break down hydroperoxides and convert them to H_2O and corresponding alcohols through a glutathione-dependent pathway, and GSH is converted to oxidized glutathione (GSSG) (Forcina & Dixon, 2019). In ferroptosis, GPx4 plays an essential role. GPx4 is the only enzyme known to prevent biofilm oxidation, promote the decomposition of hydrogen peroxide and other small molecule peroxides caused by iron homeostasis in the cells, and prevent the ROS-induced ferroptosis (Hu et al., 2019). When erastin specifically bound to GPx4 to inhibit its activity, ROS and MDA accumulated intracellularly, exhibiting ferroptosis characteristics typical of cell membrane oxidation (Fig. 5d). Yang et al (2014) reported that ferroptosis caused massive depletion of GSH, leading to inhibition of the GPx4-GSH antioxidant system and loss of endogenous cellular antioxidant capacity. However, inhibition of transit System Xc by glutamate leads to a reduction in the intracellular synthesis of precursors for GSH, resulting in the reduced GSH levels and increased GSSG levels (Fig. 4). Furthermore, incubation of erastin, a ferroptosis inducer that binds specifically to GPx4, with myocytes significantly reduced myocyte GPx activity and GSH content (Fig. 5c). Taken together, loss of GPx4 function may lead to ferroptosis in the cells.

Despite the proven action of glutathione metabolism on ferroptosis, the pathways of ABC transporters, ROS, cysteine, and methionine metabolism and glutathione metabolism were shown to interact with ferroptosis (Fig. 4h). The “Fenton response” and arachidonic (AA) dependent pathway of ferroptosis are also shown in Fig. S3. Overall, ferroptosis is dependent on the accumulation of ROS, which is not a stand-alone process, and many normal metabolic processes, including

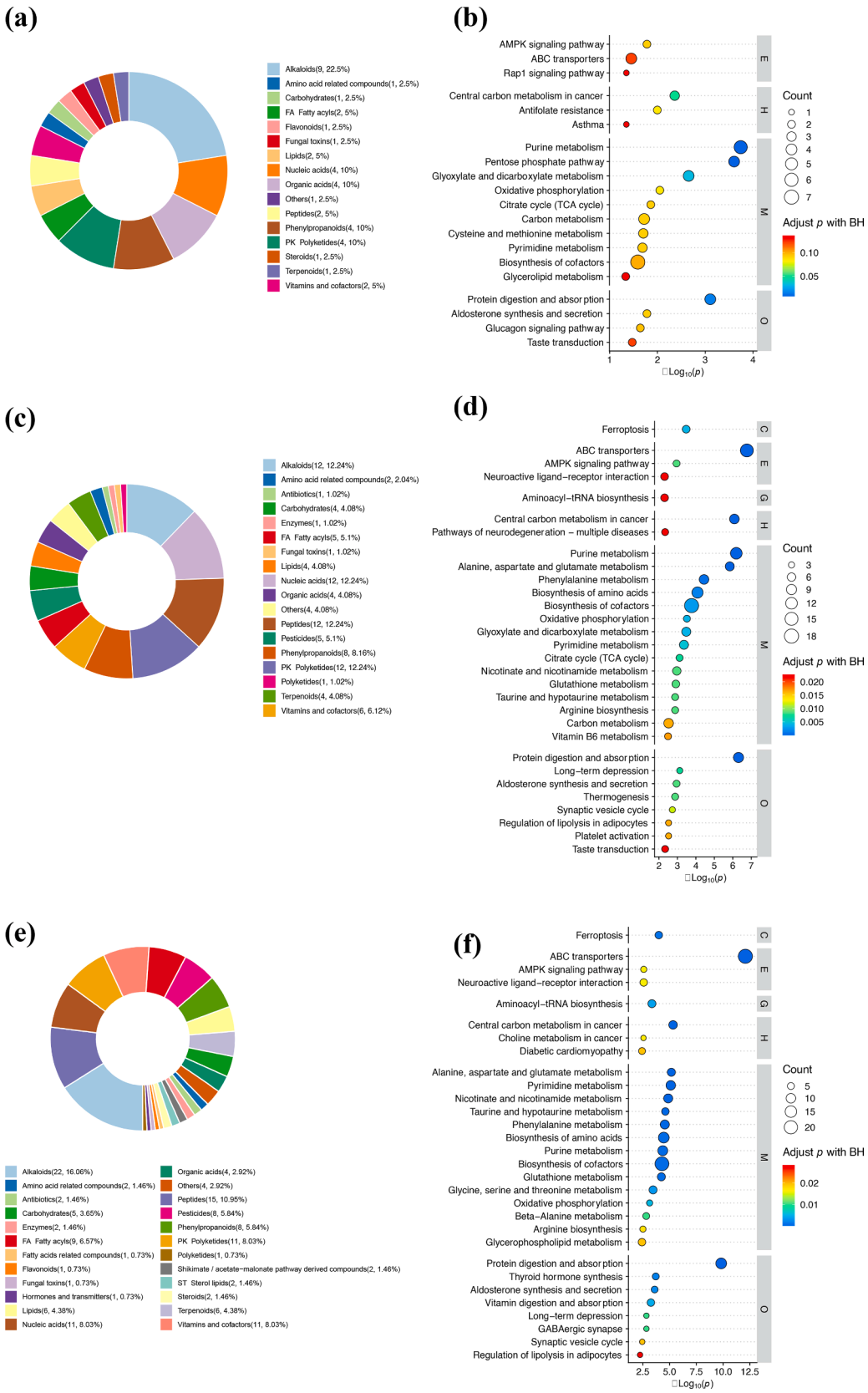

Fig. 3. (a) Classification of EXU1 and EXU2 DMs (KEGG). (b) Bubble map of EXU1 and EXU2 KEGG pathway enrichment (up to top 30). (c) Classification of EXU1 and EXU4 DMs (KEGG). (d) Bubble map of EXU1 and EXU4 KEGG pathway enrichment (up to top 30). (e) Classification of EXU1 and EXU6 DMs (KEGG). (f) Bubble map of EXU1 and EXU6 KEGG pathway enrichment (up to top 30). Pathway classification: C is cellular processes, E is environmental information processing, G is genetic information processing, H is human diseases, M is metabolism, O is organismal systems.

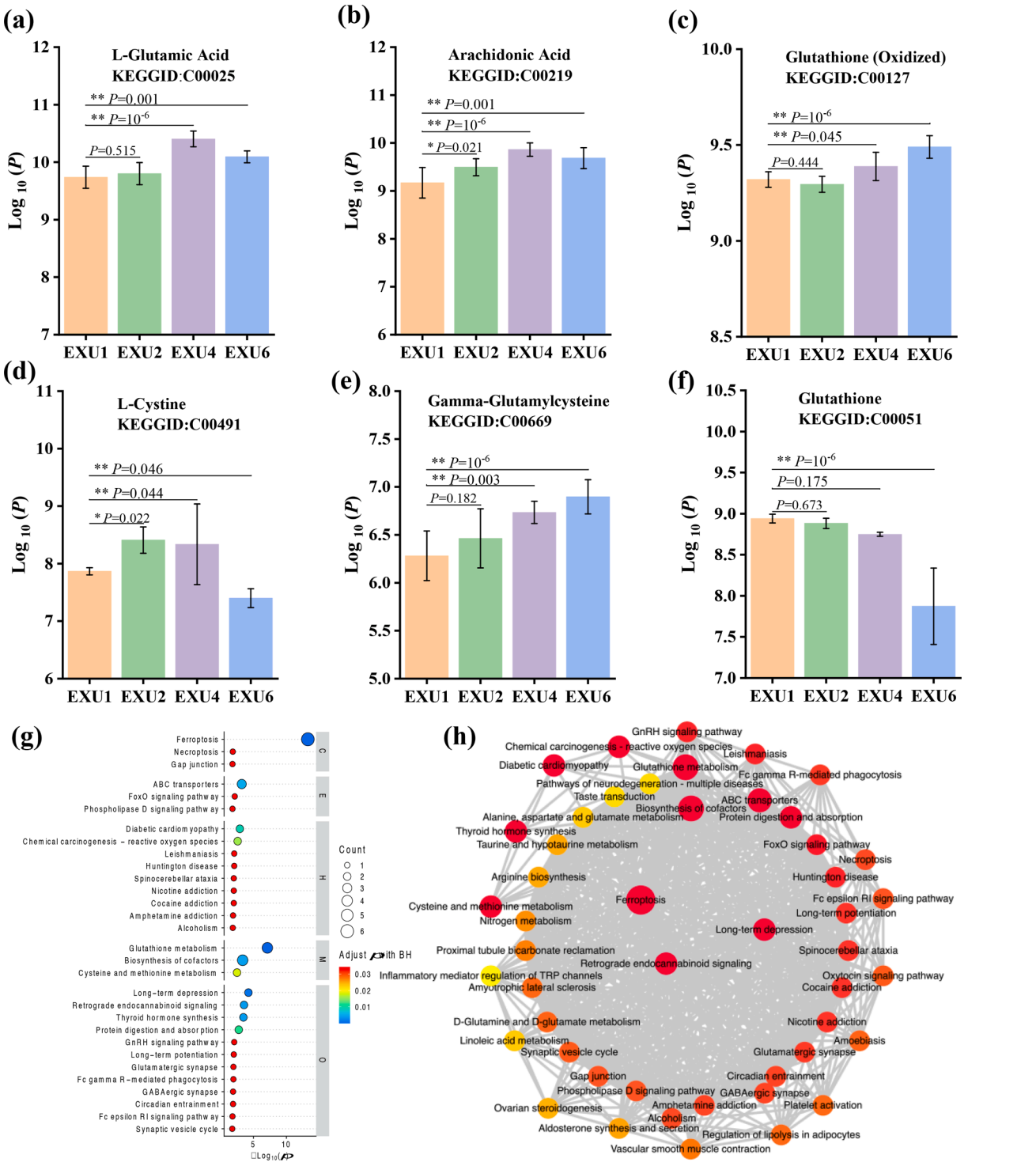

Fig. 4. (a-f) DMs involved in the cellular process of ferroptosis with KEGG ID were identified. (g) Mapping of KEGG pathway enrichment bubbles by identifying 6 DMs associated with ferroptosis (up to top 30). (h) Functional interaction networks of enriched pathways were mapped by identifying the 6 DMs associated with ferroptosis. The "*" symbol indicates a *P* value of <0.05 and the "**" symbol indicates a *P* value of <0.01. Log_{10} (*P*) indicates log operation on the ion abundance of metabolites identified by mass spectrometry. Each dot represents a pathway and the colour indicates the *P*-value of the enrichment, the shade of red indicates the enriched of the pathway.; A larger circle indicates that there are more metabolites annotated to this pathway (count); The presence of network lines between the pathways indicates that they contain common DMs, the thicker the line the more metabolites shared by the two pathways. (For interpretation of the references to colour in this figure legend, the reader is referred to the web version of this article.)

carbohydrate, amino acid, and fatty acid metabolism, mitochondrial electron transport reaction, degradation of iron-containing proteins, as well as phagocytosis (Zhang et al., 2013). The water content and water status in the muscle change in response to changes in the metabolism of the meat and the external environment (Huff-Lonergan & Lonergan, 2005). The effect of apoptosis on muscle water and its relationship with WHC have been reported (Gorska & Wojtysiak, 2018; Zhang et al., 2013). Most of the water found in the muscles is located in myofibrils, in the interstitium between myofibrils, between myocyte interstices and between muscle bundles (groups of myocyte) (Huff-Lonergan &

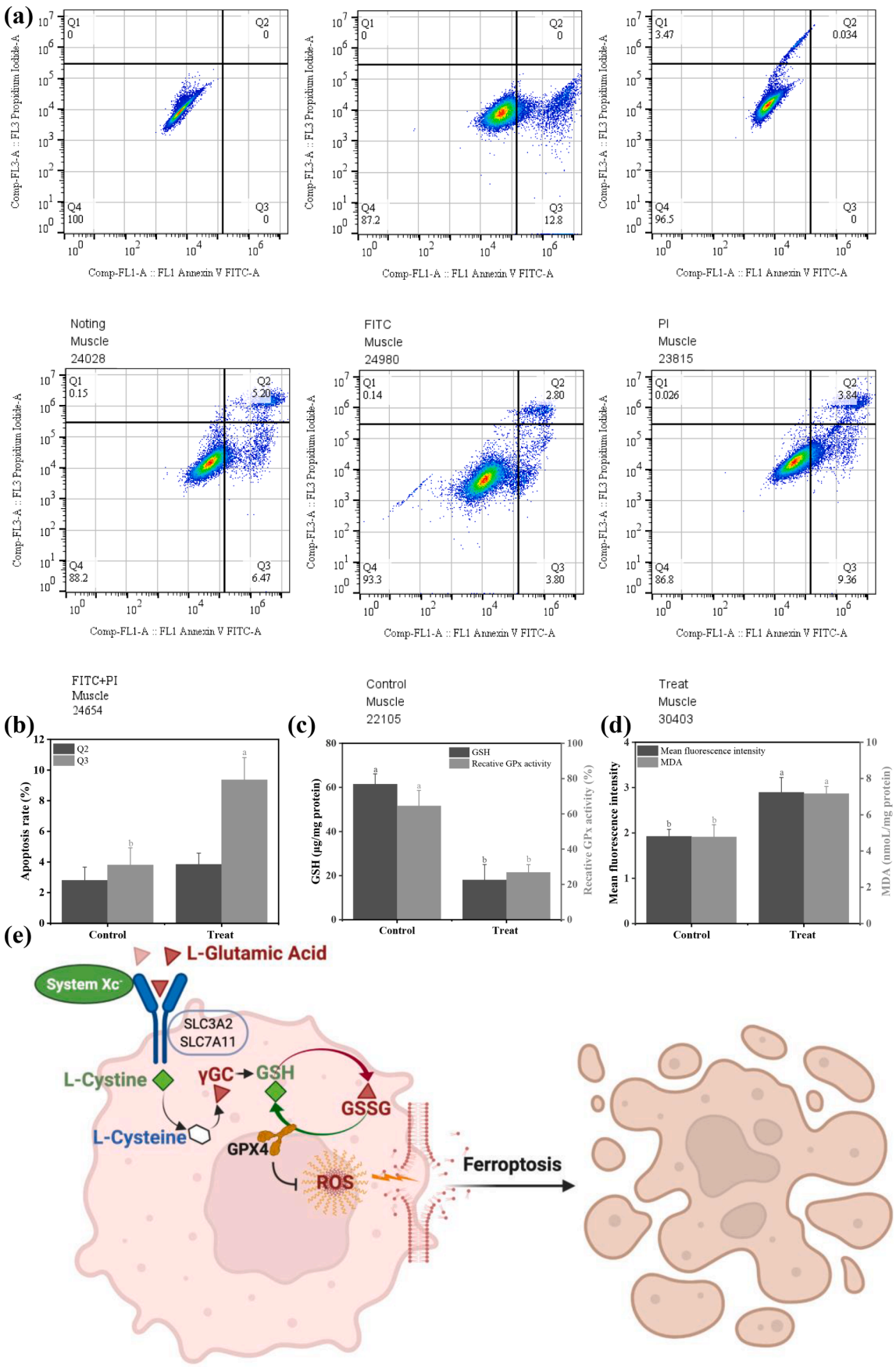

(caption on next page)

Fig. 5. (a-b) Flow cytometry was used to determine the effects of ferroptosis inducer erastin on the apoptosis of myocytes. (c) Differences in erastin-induced GSH content and GPX4 activity in myocytes; (d) Differences in erastin-induced ROS and MDA content in myocytes; (e) Schematic diagram of the molecular mechanism of ferroptosis. The KEGG ferroptosis pathway is plotted with reference to https://www.kegg.jp/kegg-bin/show_pathway?bta04216/cpd:C00025%09yellow/cpd:C00219%09yellow/cpd:C00127%09yellow/cpd:C00051%09purple/cpd:C00491%09purple/cpd:C00669%09yellow). Control, myoblast culture medium without ferroptosis inducer erastin. Treatment, myoblast culture medium was added with 10 μmol/L ferroptosis inducer erastin. The "*" symbol indicates a *P* value of <0.05 and the "**" symbol indicates a *P*-value of <0.01. Red triangle indicates upregulation, green square indicates downregulation. SLC3A2 is solute carrier family 3, member 2; SLC7A11 is solute carrier family 7 (L-type amino acid transporter), member 11; GSH, glutathione; GSH, glutathione disulfide; GPX4, phospholipid-hydroperoxide glutathione peroxidase. (For interpretation of the references to colour in this figure legend, the reader is referred to the web version of this article.)

Lonergan, 2005). Whereas the cell membrane is closely connected with the extracellular matrix *via* focal adhesions, there are network of bonds between the cells and the matrix to bind the water in the muscle tissue. When apoptosis occurs, apoptotic cells are separated from the other cells, disrupting the network structure and leading to drip loss and altering fleshy characteristics (Hou et al., 2020). In the study, analysis of the water status of beef during storage revealed that increased water loss and reduced WHC were accompanied by an increased rate of apoptosis (Fig. 1), validating the relationship between apoptosis and WHC. Thus, ferroptosis may reduce muscle WHC at specific stages during muscle aging through the apoptotic pathway.

Interestingly, we found that the core substance responsible for ferroptosis was 'ROS'. The high production of ROS is considered to be a key event in muscle-to-meat conversion, where myocytes are irritated by oxidative stress and excess ROS cannot be cleared, leading to cellular damage and the induction of autophagy and apoptosis as well as protein and lipid oxidation (Lana & Zolla, 2015). Myofibrils are rich in charged hydrophilic groups and the water binds tightly to them by capillary force, osmotic and electrostatic interaction. Protein oxidation can modify amino acid side chains, and the hydrophilic and hydrophobic areas of myofibril proteins, as well as their interaction with structural elements within and between myofibrils filaments, are altered. Cross-linking of proteins and charge on proteins are affected by these factors, thus the muscle fibers and their structure and arrangement are thereby altered, affecting the muscle WHC (Liu et al., 2022; Bao & Ertbjerg, 2019). It has been proposed by Lindahl et al. (2010) that the decrease in WHC associated with muscle aging may be due to oxidative stress-mediated protein degradation in tissue skeletal cells. Oxidative stress may affect the structure and integrity of muscle cells by increasing the amount of MetMb and O_2 available to myocyte membranes, and the muscles may be unable to absorb water, thus reducing the WHC in the meat (Bai et al., 2022; Bao & Ertbjerg, 2019). Notably, ferroptosis produces the lipid peroxide MDA, and bis-Schiff base dimine crosslinks are formed when MDA reacts with two lysine residues in proteins, myofibrillar and myoglobin molecules could potentially be oxidized through intramolecular or intermolecular protein crosslinks, which in turn promotes the release of free iron and the ferroptosis process (Liu et al., 2022; Wang, He, Emara, Gan & Li., 2019). In summary, the ferroptosis pathway affects muscle WHC through the accumulation of ROS, induction of apoptosis, and lipid and protein oxidation.

5. Conclusions

This work used metabolomics of exudates to study potential mechanisms of WHC in beef. The discovery of ferroptosis was valuable in refining the profile of apoptosis.The ferroptosis was found to be dependent on glutathione metabolism *via* the KEGG enrichment pathway analysis, followed by validation using the ferroptosis inducer erastin to induce ferroptosis in myocytes. The discovery of ferroptosis has provided a new way of thinking towards improving meat quality.

Funding

This study was financially supported by the Ningxia Natural Science Foundation (2021AAC03013-General Project; 2022AAC02021-Key Projects).

Data availability statement

Not applicable.

CRediT authorship contribution statement

Jun Liu: Conceptualization, Data curation, Formal analysis, Investigation, Methodology, Resources, Validation, Visualization, Writing – original draft, Writing – review & editing. **Ziying Hu:** Writing – review & editing. **Dunhua Liu:** Conceptualization, Formal analysis, Funding acquisition, Investigation, Project administration, Supervision, Visualization. **Anran Zheng:** Investigation. **Qin Ma:** Writing – review & editing.

Declaration of Competing Interest

The authors declare that they have no known competing financial interests or personal relationships that could have appeared to influence the work reported in this paper.

Data availability

No data was used for the research described in the article.

Acknowledgments

This work was supported by the Ningxia Natural Science Foundation (2021AAC03013, 2022AAC02021). We thank Dr. Xianghong Xie from the Northwest A&F University for his advice on writing the article. The authors would like to thank Shanghai Bioprofile Co., Ltd. for providing technical support for UPLC-ESI-Q-Orbitrap-MS metabolomics.

Appendix A. Supplementary data

Supplementary data to this article can be found online at https://doi.org/10.1016/j.foodchem.2022.133903.

References

Bai, X., Tian, W., Yin, F., Xiao, K., Chen, Q., Chai, R., Ru, A., Li, J., Zhu, C., & Zhao, G. (2022). Age-specific effect on endogenous oxidative and antioxidative characteristics of longissimus thoracis muscle of yak during early postmortem period. *Food Chemistry*, *374*, 131829-?. https://doi.org/10.1016/j.foodchem.2021.131829.

Bao, Y., & Ertbjerg, P. (2019). Effects of protein oxidation on the texture and water-holding of meat: A review. *Critical Reviews in Food Science and Nutrition, 59*, 3564–3578. https://doi.org/10.1080/10408398.2018.1498444

Bowker, B., Gamble, G., & Zhuang, H. (2016). Exudate protein composition and meat tenderness of broiler breast fillets. *Poultry Science, 95*(1), 133–137. https://doi.org/10.3382/ps/pev312

Bridges, R., Natale, N., & Patel, S. (2012). System^{xc-} cystine/glutamate antiporter: An update on molecular pharmacology and roles within the CNS. *British Journal of Pharmacology, 165*(1), 20–34. https://doi.org/10.1111/j.1476-5381.2011.01480.x

Castejón, D., García-Segura, J. M., Escudero, R., Herrera, A., & Cambero, M. I. (2015). Metabolomics of meat exudate: Its potential to evaluate beef meat conservation and aging. *Analytica Chimica ACTA, 901*, 1–11. https://doi.org/10.1016/j.aca.2015.08.032

Chen, B., Fang, L., Lin, L., Lv, Y., Huang, Z., Lin, X., & Wang, X. (2022). Aerobic exercise combined with glucosamine hydrochloride capsules inhibited the apoptosis of chondrocytes in rabbit knee osteoarthritis by affecting TRPV5 expression. *Gene*. https://doi.org/10.1016/j.gene.2022.146465, 146465.

Chen, C., Guo, Z., Ma, G., Ma, J., Zhang, Z., Yu, Q., & Han, L. (2021). Lysosomal Fe^{2+}contributes to myofibrillar protein degradation through mitochondrial-

dysfunction-induced apoptosis. *LWT, 143*, Article 111197. https://doi.org/10.1016/j.lwt.2021.111197
Cheng, Q., & Sun, D. (2008). Factors affecting the water holding capacity of red meat products: A review of recent research advances. *Critical Reviews in Food Science and Nutrition, 48*(2), 137–159. https://doi.org/10.1080/10408390601177647
Dong, L., Yang, B., Zhang, Y., Wang, S., Li, F., Xing, G., … Lu, R. (2022). Ferroptosis contributes to methylmercury-induced cytotoxicity in rat primary astrocytes and Buffalo rat liver cells. *Neurotoxicology, 90*, 228–236. https://doi.org/10.1016/j.neuro.2022.04.006
Forcina, G., & Dixon, S. (2019). GPX4 at the crossroads of lipid homeostasis and ferroptosis. *Proteomics, 19*(18), 1800311. https://doi.org/10.1002/pmic.201800311
Gorska, M., & Wojtysiak, D. (2018). Comparison of plasma corticosterone concentration, muscle fibre diameter, and apoptotic markers between normal and pale, soft, exudative (PSE) turkey breast muscles. *Medycyna Weterynaryjna-Veterinary Medicine-Science and Practice, 74*(6), 387–391. https://doi.org/10.21521/mw.6007
Hirayama, T., & Nagasawa, H. (2017). Chemical tools for detecting Fe ions. *Journal of Clinical Biochemistry and Nutrition, 60*(1), 39–48. https://doi.org/10.3164/jcbn.16-70
Hou, X., Liu, Q., Meng, Q., Wang, L., Yan, H., Zhang, L., & Wang, L. (2020). TMT-based quantitative proteomic analysis of porcine muscle associated with postmortem meat quality. *Food Chemistry, 328*, Article 127133. https://doi.org/10.1016/j.foodchem.2020.127133
Hu, C., Nydes, M., Shanley, K., Pantoja, I., Howard, T., & Bizzozero, O. (2019). Reduced expression of the ferroptosis inhibitor glutathione peroxidase-4 in multiple sclerosis and experimental autoimmune encephalomyelitis. *Journal of Neurochemistry, 148*(3), 426–439. https://doi.org/10.1111/jnc.14604
Huff-Lonergan, E., & Lonergan, S. M. (2005). Mechanisms of water-holding capacity of meat: The role of postmortem biochemical and structural changes. *Meat Science, 71*(1), 194–204. https://doi.org/10.1016/j.meatsci.2005.04.022
Karakaya, M., Saricoban, C., & Yilmaz, M. T. (2005). The effect of various types of poultry pre- and post-rigor meats on emulsification capacity, water-holding capacity and cooking loss. *European Food Research and Technology, 220*(3), 283–286. https://doi.org/10.1007/s00217-004-1068-1
Kim, G., Jung, E., Lim, H., Yang, H., Joo, S., & Jeong, J. (2013). Influence of meat exudates on the quality characteristics of fresh and freeze-thawed pork. *Meat Science, 95*(2), 323–329. https://doi.org/10.1016/j.meatsci.2013.05.007
Kristensen, L., & Purslow, P. P. (2001). The effect of ageing on the water-holding capacity of pork: Role of cytoskeletal proteins. *Meat Science, 58*(1), 17–23. https://doi.org/10.1016/S0309-1740(00)00125-X
Lana, A., & Zolla, L. (2015). Apoptosis or autophagy, that is the question: Two ways for muscle sacrifice towards meat. *Trends in Food Science & Technology*, *46*(2, Part A), 231-241. https://doi.org/10.1016/j.tifs.2015.10.001.
Lindahl, G., Lagerstedt, Å., Ertbjerg, P., Sampels, S., & Lundström, K. (2010). Ageing of large cuts of beef loin in vacuum or high oxygen modified atmosphere - Effect on shear force, calpain activity, desmin degradation and protein oxidation. *Meat Science, 85*, 160–166. https://doi.org/10.1016/j.meatsci.2009.12.020
Li, X., Wei, X., Wang, H., Zhang, C., & Mehmood, W. (2018). Relationship between protein denaturation and water holding capacity of pork during postmortem ageing. *Food Biophysics, 13*, 18–24. https://doi.org/10.1007/s11483-017-9507-2
Liu, J., Liu, D., Wu, X., Pan, C., Wang, S., & Ma, L. (2022). TMT quantitative proteomics analysis reveals the effects of transport stress on iron metabolism in the liver of chicken. *Animals, 12*(1), 52. https://doi.org/10.3390/ani12010052
Mehta, A., Prabhakar, M., Kumar, P., Deshmukh, R., & Sharma, P. L. (2013). Excitotoxicity: Bridge to various triggers in neurodegenerative disorders. *European Journal of Pharmacology, 698*(1), 6–18. https://doi.org/10.1016/j.ejphar.2012.10.032
Pitman, K., Alluri, S., Kristian, A., Aarnes, E., Lyng, H., Riss, P., & Malinen, E. (2019). Influx rate of F-18-fluoroaminosuberic acid reflects cystine/glutamate antiporter expression in tumour xenografts. *European Journal of Nuclear Medicine and Molecular Imaging, 46*(10), 2190–2198. https://doi.org/10.1007/s00259-019-04375-8
Wang, Z., He, Z., Emara, A. M., Gan, X., & Li, H. (2019). Effects of malondialdehyde as a byproduct of lipid oxidation on protein oxidation in rabbit meat. *Food Chemistry, 288*, 405–412. https://doi.org/10.1016/j.foodchem.2019.02.126
Wang, H., Liu, C., Zhao, Y., & Gao, G. (2020). Mitochondria regulation in ferroptosis. *European Journal of Cell Biology, 99*(1), e202105043.
Xia, J., Si, H., Yao, W., Li, C., Yang, G., Tian, Y., & Hao, C. (2021). Research progress on the mechanism of ferroptosis and its clinical application. *Experimental Cell Research, 409*(2), Article 112932. https://doi.org/10.1016/j.yexcr.2021.112932
Xing, T., Zhao, X., Xu, X., Li, J., Zhang, L., & Gao, F. (2020). Physiochemical properties, protein and metabolite profiles of muscle exudate of chicken meat affected by wooden breast myopathy. *Food Chemistry, 316*, Article 126271. https://doi.org/10.1016/j.foodchem.2020.126271
Xu, R., Huang, Y., Zhu, D., & Guo, J. (2022). Iron promotes Slc7a11-deficient valvular interstitial cell osteogenic differentiation: A possible mechanism by which ferroptosis participates in intraleaflet hemorrhage-induced calcification. *Free Radical Biology and Medicine, 184*, 158–169. https://doi.org/10.1016/j.freeradbiomed.2022.03.013
Yang, W. S., SriRamaratnam, R., Welsch, M. E., Shimada, K., Skouta, R., Viswanathan, V. S., … Stockwell, B. R. (2014). Regulation of ferroptotic cancer cell death by GPX4. *Cell, 156*(1–2), 317–331. https://doi.org/10.1016/j.cell.2013.12.010
Yang, W. S., & Stockwell, B. R. (2016). Ferroptosis: Death by lipid peroxidation. *Trends in Cell Biology, 26*(3), 165–176. https://doi.org/10.1016/j.tcb.2015.10.014
Zhang, M., Wang, D., Huang, W., Liu, F., Zhu, Y., Xu, W., & Cao, J. (2013). Apoptosis during postmortem conditioning and its relationship to duck meat quality. *Food Chemistry, 138*(1), 96–100. https://doi.org/10.1016/j.foodchem.2012.10.142
Zhang, M., Wang, D., Xu, X., & Xu, W. (2019). Comparative proteomic analysis of proteins associated with water holding capacity in goose muscles. *Food Research International, 116*, 354–361. https://doi.org/10.1016/j.foodres.2018.08.048

Further reading

Liu, J., Liu, D., Zheng, A., & Ma, Q. (2022). Haem-mediated protein oxidation affects water-holding capacity of beef during refrigerated storage. *Food Chemistry: X, 100304*. https://doi.org/10.1016/j.fochx.2022.100304
Zhang, W., Xiao, S., & Ahn, D. (2013). Protein Oxidation: Basic Principles and Implications for Meat Quality. *Critical Reviews in Food Science and Nutrition, 53*(11), 1191–1201. https://doi.org/10.1080/10408398.2011.577540